Electronic Supplementary Information

For

Interpretable Molecular Models for Molybdenum Disulfide and Insight into Selective Peptide Recognition

Juan Liu[1], Jin Zeng[1], Cheng Zhu[1], Jianwei Miao[2,3], Yu Huang[3,4], Hendrik Heinz[1*]

[1] Department of Chemical and Biological Engineering, University of Colorado-Boulder, Boulder, CO 80309, USA

[2] Department of Physics and Astronomy, University of California Los Angeles, California 90095, USA

[3] California NanoSystems Institute, University of California, Los Angeles, CA 90095, USA

[4] Department of Materials Science and Engineering, University of California, Los Angeles, 90095, USA

[*] Corresponding author: hendrik.heinz@colorado.edu

Table of Contents

S1. Computational and Experimental Details

S1.1. Construction of Molecular Models. Materials Studio[1] was employed to build all-atom models of the 2H-MoS_2 surface, the peptides Y, T, T7 and water (TIP3P and flexible SPC). We utilized the unit cell of 2H-MoS_2 by Wyckoff (database_code_amcsd 0011823)[2] and also created an identical orthorhombic supercell (γ=90º) from two hexagonal supercells (γ=120º), which is helpful for running simulations with rectangular MoS_2 model surfaces, for example, using the NAMD program. The protonation state of the peptides was adjusted to represent neutral conditions as in experiment (pH $\simeq$7). All simulation systems were charge-neutral. Initial conformations for the peptides were chosen from molecular dynamics simulation of the peptides in water using the CHARMM36 force field.[3] We then carried out annealing at 600 K for 5 ns, then cooled down to room temperature, and carried out MD simulations in the NPT ensemble for a further period of 5 ns at 298.15 K and 101.3 kPa. Annealing helped in conformation sampling and overcoming rotation barriers for the single peptides within shorter simulation time.

S1.2. Simulation Protocol. Molecular dynamics simulations were carried out in the NPT ensemble using the Nanoscale Molecular Dynamics program (NAMD)[4], as well as the Discover program in Materials Studio (mostly for short tests), using a time step of 1 fs. All atoms were allowed to move freely. The temperature was controlled at 298.15 K with the velocity scaling and a temperature window of 10 K (Discover), or with the Langevin thermostat and a damping coefficient of 1 ps^{-1} (NAMD). A spherical cutoff of 12 Å for van-der-Waals interactions was applied for the summation of pair-wise Lennard-Jones interactions. The summation of Coulomb interactions was carried out using the Particle Mesh Ewald (PME) method with a high accuracy of 10^{-6} kcal/mol throughout all

equilibration and production runs. The average temperature generally remained within ±0.35 K of the target temperature, however, instantaneous temperature fluctuations were in a range of ±10 K.

S1.3. Calculation of Lattice Parameters and X-ray Diffraction (XRD) Pattern. Specifically, the lattice parameters were calculated in the NPT ensemble using three-dimensional periodical boundary conditions, temperature control by velocity scaling, Ewald summation for Coulomb interactions in high accuracy of 10^{-6} kcal/mol, and a 12 Å cutoff for van der Waals interactions. Snapshots were taken every 200 fs for a duration of 50 to 100 ps to obtain deviations in block averages lower than 0.1%. The XRD pattern was computed from the equilibrium structure of an MoS_2 supercell using the Reflex module (Powder diffraction) in Materials Studio. A constant isotropic pressure of 1.013 MPa and a temperature of 298.15 K were applied.

S1.4. Calculation of Vibration Spectra. The (4×4×2) supercell was used as the initial structure to determine the superposition of Infrared (IR) and Raman spectra using molecular dynamics simulation. We started with an equilibrium structure and 1 ps equilibration in the NVT ensemble, followed by a 5 ps NPT simulation. Snapshots were then collected every 5 fs. Then, the velocity autocorrelation function (VACF) was calculated for all atoms and subjected to a Fourier transform to yield the vibration spectrum.

For further comparison, we utilized DFT calculations with the revised PBE density functional to compute an IR spectrum. We started with an energy minimization up to 100 cycles and then proceeded with the calculation of vibration frequencies. We utilized an

ultrafine energy cutoff of 720 eV and a fine k-point set with norm-conserving pseudopotentials. The program CASTEP was employed.

S1.5. Calculation of Bulk Modulus and Young's Modulus. The mechanical properties (bulk modulus and Young's modulus) were calculated with the Forcite module of Materials Studio using the open force field format (.off) file. Reported bulk and Young's moduli are an average from 10 equilibrium conformation randomly collected from 50 ps NPT simulation at low strain (under 1%). The uncertainty was obtained from the standard deviations of the 10 individual computations.

S1.6. Calculation of Compressive Modulus. The compressibility was analyzed under different pressures (0.001, 1, 1.5, 2, 3, 4 Kbars) using simulations of 100 ps duration in the NPT ensemble at 298.15 K. A (4×4×2) supercell is used as the simulation model and the volume change was recorded. The final compression curve is a function of volume change portion ($\Delta V/V_0$) versus pressure (P). CVFF parameters were employed, along with a spherical cutoff of 12 Å for Lennard-Jones interactions, high accuracy electrostatics (Ewald method with 10^{-6} accuracy), and a time step of 1 fs. Temperature and pressure were controlled by velocity scaling (temperature window 10 K) and by the Parrinello-Rahman method, respectively.

S1.7. Calculation of Cleavage Energy. The cleavage energy $E_{cleavage}$ was calculated by using the Discover program in Material Studio with different energy expressions (CVFF, PCFF, CHARMM, AMBER, OPLS-AA) (Figure 4). It is equal to the difference in average energy of slab and bulk models (Figure 4a, b). The cross-sectional area was 32.844×37.925 $Å^2$. A hexagonal supercell yielded the same values as the rectangular surface, provided the layer thickness is at least 2 nm. The bulk models were first relaxed

over a period of 30 ps in the NPT ensemble under 298.15 K and 1.013 MPa. Then the corresponding slab surfaces were created by insertion of a 40 Å vacuum slab. These bulk and slab models were next subjected to molecular dynamics simulation in the NVT ensemble for a simulation time of 6 ns with a time step of 1 fs at 298.15 K. The first 3 ns were utilized to equilibrate the structures. Block-average energies during the last 3 ns simulation time was used to calculate $E_{cleavage}$. The computed cleavage energy for different force fields is quite closely the same, around 147 mJ/m^2 (Table S4). The error was determined from the average uncertainties during three independent simulations.

S1.8. Calculation of Contact Angle. The contact angles were computed using MD simulation of solvent molecules (1184 water and 140 diiodomethane respectively) in the NVT ensemble at 298.15 K on a 197×31.6 $Å^2$ (water) or 241×31.6 $Å^2$ (diiodomethane) MoS_2 surfaces. The initial solvent molecules with the same dimension in y axis were placed in the middle of the surface which allow the spreading of solvent molecules along x axis and avoid interactions with periodic images (Figure S2b and c). The TIP3P water model was employed to calculate the water contact angle. The total simulation time was 10 ns, of which the first 5 ns served for equilibration and the last 5 ns were used to collect data. The obtained trajectory files were visualized using the VMD graphical interface.[5] Contact angles were then graphically measured from the rendered images according to a new circle-based method (Figure S2). Average contact angles are reported from 100 snapshots and as an average over three independent runs. If using the flexible SPC water model instead, the contact angles remained the same within 1° deviation.

S1.9. Setup of Molecular Dynamics Simulations and Calculation of Adsorption Energies. The simulation of equilibrium conformations and adsorption energies of single

peptides on MoS_2 surfaces involved two simulation boxes for each peptide-MoS_2 combination, and multiple replicas thereof. The models contained (1) surface-water-peptide with the peptide 40 Å away from the surface, (2) surface-peptide-water with the peptide about 3 Å away from the surface. The total number of atoms, total volume, and box dimensions were the same in calculations (1) and (2). The box dimensions were 54.74×56.89×100 $Å^3$ initially in both cases, changing to 54.73 × 56.91 × 96.8 $Å^3$ in equilibrium, and the surface coverage was between 8% and 20%. The water portion consisted of 2000 explicit water molecules in each box using TIP3P model. Alternatively, using the flexible SPC water model would hardy affect the results. Peptides YSATFTY, TSHMSNT, YIPHTPN, and T7 were capped with N-terminal acylation and C-terminal amidation as in the experiments.[6] For the backbone GGGGGGG, the terminals are $-COO^-$ and $-NH_3^+$ as expected at pH 7. The CHARMM36-INTERFACE force field with the new MoS_2 parameters was used. The peptides were represented by CHARMM36 parameters, respectively.[3] Adsorption energies were computed as follows:

$$E_{ads} = E_2 - E_1 \quad \text{(S1)}$$

For each box, three independent NPT simulation at room temperature were performed for 10 ns after a brief energy minimization. To accurately compute relatively small differences between large total energies of two simulation boxes and extract the adsorption energies, the average total energies of individual boxes were corrected to the exact target temperature of 298.15 K using the heat capacity of each system. Arrival at steady state was determined from the convergence of the total energy at a steady value, and only this portion of the trajectory was used for analysis (i.e., the initial parts of the trajectories were discarded). The reported uncertainty is the average uncertainty of three simulation results.

S1.10. Analysis of Conformations and Molecular Dynamics Simulations of Peptide Adsorption. The conformations of the peptides were visually analyzed before and after adsorption on the MoS_2 surface. The average number of water molecules displaced by the peptides upon adsorption was determined within 3.5 Å distance above the MoS_2 surface atomic layer, which corresponds to the typical distance of the first layer of water molecules in contact with the MoS_2 surface.

The percentage of contact time for each residue was measured as the ratio of the number of snapshots in which any atom of the residue was located within 3.5 Å from the MoS_2 surface and the total number of snapshots in equilibrium. Hereby, the entire simulation time with at least 200 snapshots in equilibrium was employed. The Python package MDTraj[7] was used to read information of the atom positions in the trajectory file, and the Python script is available as part of the ESI.

S1.11. Uncertainty and Reproducibility of Simulations. The uncertainty of the simulations is low for the nanoscale systems studied, shown by deviations in the sub-% range for lattice parameters and of only few percent for several other properties relative to experimental data. Refinements of van-der-Waals parameters (σ) for the sulfur atom relative to an initial study focused on experimental data were made.[8] The interaction of the peptide YSATFTY with the MoS_2 surface was earlier reported as -96±9 kcal/mol[8] and is now -86±6 kcal/mol (see Section S3). Uncertainties related to the force field parameters are less than half this difference, i.e., approximately 5% in adsorption energies.

S1.12. Determination of the Order of Peptide Binding Affinity to MoS_2 Surfaces in Experiments. The qualitative comparison of peptide binding affinity (YSATFTY, TSHMSNT, YIPHTPN) to the MoS_2 surfaces was based on the relative affinity after

several washing cycles in biopanning experiments. The experiments were performed using the M13 phage display library from New England Biolabs as previously described.[8, 9]

S2. Additional Details of Energy Expressions

The major difference between the two energy expressions in equations (1) and (2) is the nonbonded portion so that $\sigma_{0,ii}$ and $\varepsilon_{0,ii}$ need to be evaluated independently (Table 2). Lennard-Jones parameters for PCFF using a 9-6 LJ potential differ slightly from the LJ parameters for CVFF, CHARMM, AMBER and OPLS-AA using a 12-6 LJ potential related to weaker repulsive forces in the 9-6 form. Atomic charges represent internal dipoles and multipoles and remain the same for all energy expressions.[10] Equilibrium bond lengths and bond angles are taken from X-ray data and not adjustable, or only within few percent to account for contributions by nonbond interactions. The parameters for bond stretching and angle bending are also the same, or nearly the same (in case of OPLS-AA), for all energy expressions regardless of 12-6 or 9-6 Lennard-Jones potentials. Some differences in scaling of nonbond interactions between 1, 4 bonded atoms in OPLS-AA (0.5 vdW, 0.5 Coulomb) and AMBER (0.5 vdW, 5/6 Coulomb) relative to the other force fields (1.0 for vdW and Coulomb) required a small adjustment for OPLS-AA. Differences in combination rules for 12-6 LJ parameters (arithmetic mean of $\varepsilon_{0,ii}$ in CHARMM and AMBER versus geometric mean in CVFF and OPLS-AA) were of negligible influence for MoS_2. Molecular dynamics simulations were carried out by using the parameters in equations (1) and (2).

S3. Prior Computation of YSATFTY Adsorption Energy

In ref. [8], an adsorption energy of -96 ±9 kcal/mol was reported for the adsorption of a single peptide YSATFTY on MoS_2. Here, we report -86±6 kcal, which we consider more accurate. The difference is related to better understanding and interpretation of the parameters. In ref. [8], an initial version of the force field was used with a sigma value in the Lennard-Jones function of 385 pm. For the final force field reported here, this value was changed to 384 pm, which better reproduces the cleavage energy and IR/Raman spectrum. All other force field parameters are identical. The adsorption energies for YSATFTY reported in ref. [8] still agree within the reported error bars. In addition, the adsorption energy is sensitive to the surface coverage and conformation sampling.

S4. Supplementary Figures and Tables

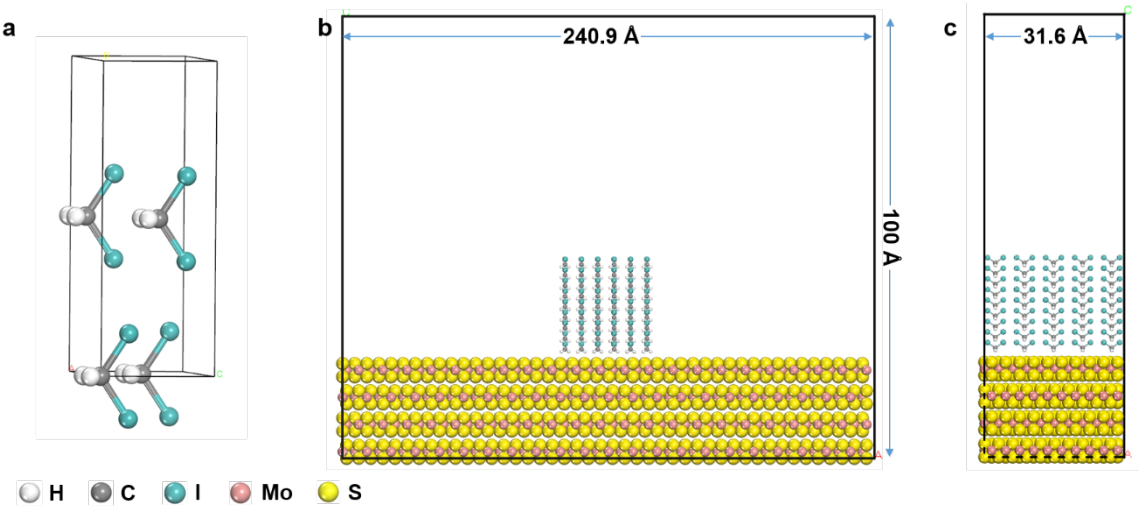

Figure S1. Schematic of model setup to compute the contact angle of diiodomethane (CH_2I_2) on the MoS_2 surface. (a) Model of CH_2I_2 unit cell. (b) x-z sideview and (c) y-z

sideview of the start structure to compute the CH_2I_2 contact angle using a cylindrically shaped liquid phase.

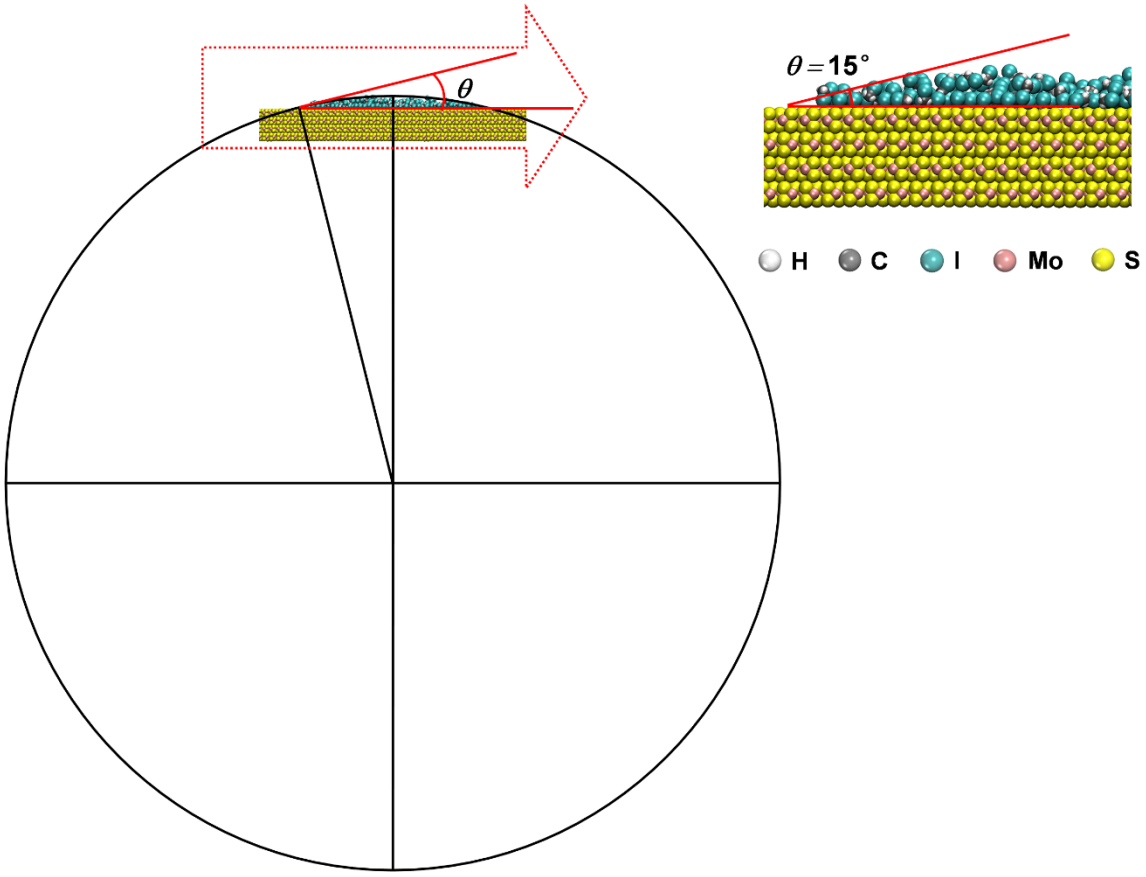

Figure S2. A new method to accurately measure the contact angle of liquids on solid surfaces in molecular dynamics simulations. The example of CH_2I_2 on the 2H-MoS_2 surface is shown, using an equilibrium trajectory of 10 ns MD simulation at 298.15 K in the NVT ensemble. The method allows up to ±1° accuracy in comparison to ±5° uncertainty with earlier methods. The panel on the right is a partial, magnified image of the snapshot fitted into a circle on the left.

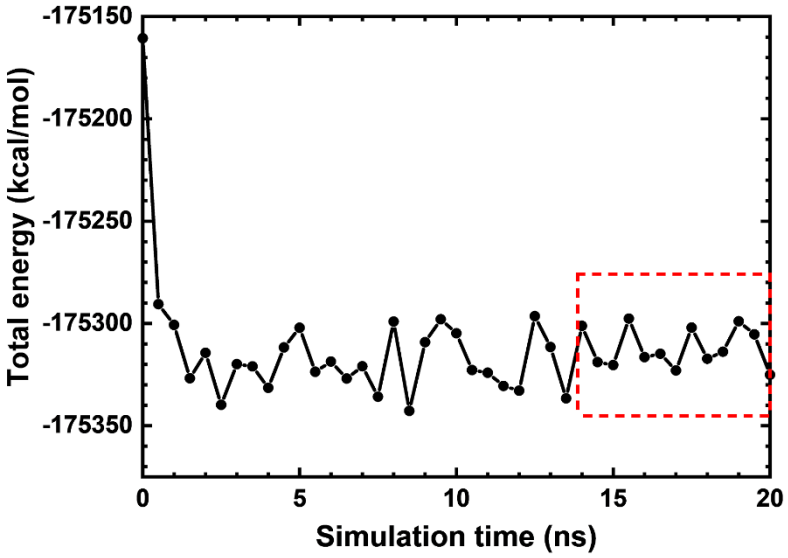

Figure S3. Method used to determine the equilibrium state of peptide adsorption on MoS_2 surfaces, as well as for equilibration of peptide conformations in solution. Energies were analyzed using block average values with a block size of 0.5 ns over the entire simulation. The initial drift in average energy and in lattice parameters subsided after ~2 ns, however, water molecules continued to show notable exchange motion near the surface. The equilibrium state highlighted (red dashed box) was determined at a time when the block-average energy had an amplitude less than 0.01% of the total energy and lasted at least 4 ns.

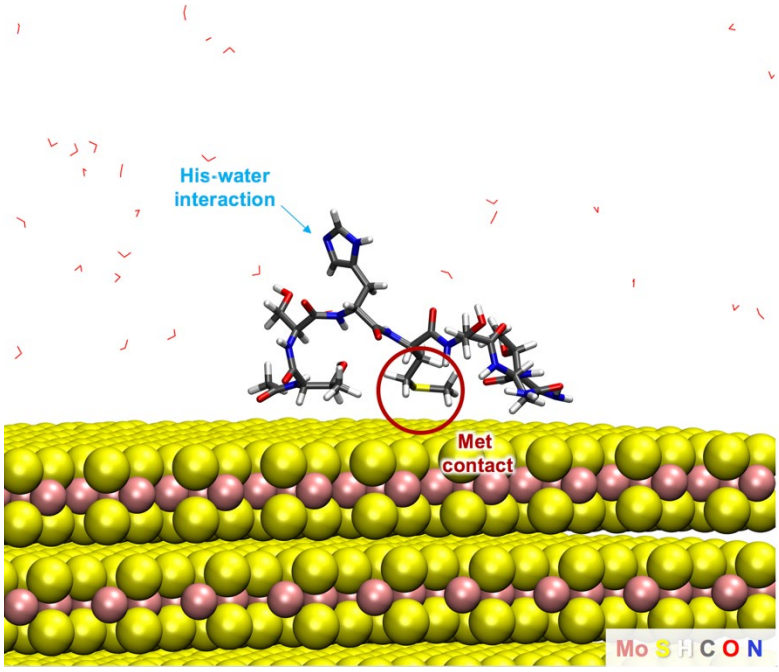

Figure S4. Side views of adsorbed conformations of TSHMSNT in equilibrium, including highlights of Met and His binding features.

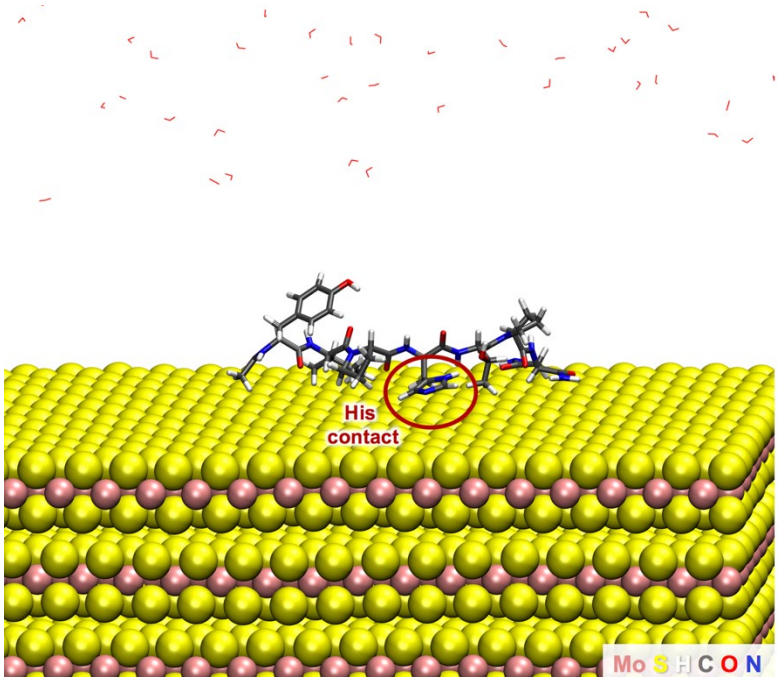

Figure S5. Side views of adsorbed conformations of YIPHTPN in equilibrium, including highlights His surface contact. However, His at pH >7 tends to be a weak binder or a non-binder as it is often attracted to solution (as in TSHMSNT).

Table S1. Current and previous potential functions used for MoS_2 in different force fields as listed in Table 1.

Method	Energy function*		
	Bond	Angle	Non-bond
IFF	Harm.	Harm.	Coul.+LJ
SR(2017)[11]	Harm.	Harm.	Coul.+LJ
LU(2016)[12]	-	-	Coul.+LJ
JI(2013)[13]	Stillinger-Weber potential		
DA(2012)[14]	-	-	Coul.+LJ
VA9(2010)[15]	Harm.	Harm.	Coul.+LJ
VA8(2010)[15]	Mors.	Harm.	Coul.+LJ
LI(2009)[16]	REBO potential		LJ
ON(2009)[17]	Harm.	Harm.	Coul.+Buck.
MO(2008)[18]	Harm.	Harm.	Coul.+Buck.
BE(2003)[19]	Mors.	Harm.	Coul.+LJ
FA(1996)[20]	Harm.	Cos.	Coul.+LJ
BR(1992)[21]	Harm.	Harm.	LJ
DR(1988)[22]	Harm.	Harm.	LJ

*Abbreviations and potential function

Terms	Definition	Potential function
Harm.	Harmonic potential	$E_{bond} = \sum_{\substack{i\in Mo \\ j\in S}} k_{bond}\left(r_{ij} - r_0\right)^2$ $E_{angle} = \sum k_\alpha(\alpha - \alpha_0)^2$
Cos.	Cosine angle potential	(1) Cosine-squared $E_{Mo-S-Mo} = \sum_\emptyset k_\emptyset[\cos(\emptyset) - \cos(\emptyset_0)]^2$ (2) Cosine-periodic $E_{S-Mo-S} = \sum_{\alpha=\theta,\omega,\psi} k_\alpha[1 - \cos(4\alpha)]$
Mors.	Morse potential	$E_{bond} = \sum_{\substack{i\in Mo \\ j\in S}} D_{ij}\{1 - e^{[-\alpha_{ij}(r_{ij} - r_{ij,0})]}\}^2$
Coul.	Coulomb potential	$E_{coul} = \sum_{\substack{i,j\in Mo,S \\ i\neq j}} \frac{1}{4\pi\varepsilon_0}\frac{q_i q_j}{r_{ij}}$
LJ	Lennard-Jones potential	$E_{LJ} = \sum_{\substack{i,j\in Mo,S \\ i\neq j}} 4\varepsilon_{ij}[(\frac{\sigma_{ij}}{r_{ij}})^{12} - \left(\frac{\sigma_{ij}}{r_{ij}}\right)^6]$
Buck.	Buckingham potential	(1) $E_{buck} = \sum_{\substack{i,j\in Mo,S \\ i\neq j}} A_{ij} e^{(\frac{\sigma_{ij} - r_{ij}}{\rho_{ij}})}$, in MO (2008). (2)$E_{buck} = \sum_{\substack{i,j\in Mo,S \\ i\neq j}} A_{ij} e^{(\frac{\sigma_{ij} - r_{ij}}{\rho_{ij}})} - \frac{C_{ij}}{r_{ij}^6}$, in ON (2009).
ER	Extended reactive empirical bond-order (REBO) potential	See ref. [16]
SW	Stillinger-Weber potential	See ref. [13]

Table S2. The angle section of the CHARMM parameters for 2H-MoS_2. The complete CHARMM force field file is shared as part of the ESI.

Angle types	***symbol***	K_θ **(kcal·mol^{-1}·rad^{-2})**	$\theta_{0,\,ijk}$ **(°)**
S1-MO1-S1	θ_1	205.0	84.32
S1-MO1-S2	θ_1	205.0	84.32
S1-MO1-S3	θ_2	0.0	78.38
S1-MO1-S4	θ_3	3.6	134.40
S1-MO2-S1	θ_1	205.0	84.32
S1-MO2-S2	θ_1	205.0	84.32
S1-MO2-S3	θ_5	3.6	78.38
S1-MO2-S4	θ_3	3.6	134.40
S2-MO1-S2	θ_1	205.0	84.32
S2-MO1-S3	θ_3	3.6	134.40
S2-MO1-S4	θ_5	3.6	78.38
S2-MO2-S2	θ_1	205.0	84.32

S2-MO2-S3	θ_3	3.6	134.40
S2-MO2-S4	θ_2	0.0	78.38
S3-MO1-S3	θ_1	205.0	84.32
S3-MO1-S4	θ_1	205.0	84.32
S3-MO2-S3	θ_1	205.0	84.32
S3-MO2-S4	θ_1	205.0	84.32
S4-MO1-S4	θ_1	205.0	84.32
S4-MO2-S4	θ_1	205.0	84.32
MO1-S1-MO2	θ_4	205.0	84.32
MO1-S2-MO2	θ_4	205.0	84.32
MO1-S3-MO2	θ_4	205.0	84.32
MO1-S4-MO2	θ_4	205.0	84.32
MO1-S1-MO1	θ_4	205.0	84.32
MO1-S2-MO1	θ_4	205.0	84.32
MO1-S3-MO1	θ_4	205.0	84.32

MO1-S4-MO1	θ_4	205.0	84.32
MO2-S1-MO2	θ_4	205.0	84.32
MO2-S2-MO2	θ_4	205.0	84.32
MO2-S3-MO2	θ_4	205.0	84.32
MO2-S4-MO2	θ_4	205.0	84.32

Table S3. Revised CVFF parameters for diiodomethane (DIM) and validation. The same parameters can be used in CHARMM.

I. Nonbond	**Charge (e)**	**σ (pm)**	**ε (kcal·mol^{-1})**
C	-0.086	400	0.032
H	+0.09	268	0.045
I	-0.047	438	0.750
II. Bond	**$r_{0,ij}$ (pm)**		**K_r (kcal·mol^{-1}·Å^{-2})**
C-H	111.1		309
C-I	215.0		90
III. Angles	**$\theta_{0,ijk}$ (°)**		**K_θ (kcal·mol^{-1}·rad^{-2})**
I-C-I	112.96		95
I-C-H	108.37		28
H-C-H	110.40		35
IV. Validations	**Computation**		**Experiment** [23]
Dipole moment (Debye)	1.083		1.08
Density (g/cm^3)	3.35±0.03		3.325
Vaporization energy (kJ/mol)	44±2		42.5

Table S4. The cleavage energy of 2H-MoS_2 estimated from experiments, quantum mechanics, and molecular dynamics simulations using IFF with different energy expressions at 298 K (CVFF, PCFF, CHARMM, AMBER, OPLS-AA).

Method	**Cleavage energy (mJ/m^2)**
Expt[24]	99~121
Quantum mechanics - DFT[25-27]	160-284
Estimated best reference from expt and DFT	150±10
IFF-CVFF	149±2
IFF-PCFF	148±2
IFF-CHARMM	150±2
IFF-AMBER	144±8
IFF-OPLS-AA	146±7

Supplementary References

1. *Accelrys Inc., San Diego, CA*, 2011.
2. R. W. G. Wyckoff, *Crystal Structures*, Interscience Publishers, New York, 2nd edn., 1963.
3. R. B. Best, X. Zhu, J. Shim, P. E. Lopes, J. Mittal, M. Feig and A. D. MacKerell Jr, *J. Chem. Theory Comput.*, 2012, **8**, 3257-3273.
4. J. C. Phillips, R. Braun, W. Wang, J. Gumbart, E. Tajkhorshid, E. Villa, C. Chipot, R. D. Skeel, L. Kale and K. Schulten, *J. Comput. Chem.*, 2005, **26**, 1781-1802.
5. W. Humphrey, A. Dalke and K. Schulten, *J. Mol. Graphics*, 1996, **14**, 33-38.
6. P. Li, K. Sakuma, S. Tsuchiya, L. Sun and Y. Hayamizu, *ACS Appl. Mater. Interfaces*, 2019, **11**, 20670-20677.
7. R. T. McGibbon, K. A. Beauchamp, M. P. Harrigan, C. Klein, J. M. Swails, C. X. Hernández, C. R. Schwantes, L.-P. Wang, T. J. Lane and V. S. Pande, *Biophys. J.*, 2015, **109**, 1528-1532.
8. J. Chen, E. Zhu, J. Liu, S. Zhang, Z. Lin, X. Duan, H. Heinz, Y. Huang and J. J. De Yoreo, *Science*, 2018, **362**, 1135-1139.
9. C.-Y. Chiu, Y. Li, L. Ruan, X. Ye, C. B. Murray and Y. Huang, *Nat. Chem.*, 2011, **3**, 393-399.
10. H. Heinz and U. W. Suter, *J. Phys. Chem. B*, 2004, **108**, 18341-18352.
11. V. Sresht, A. Govind Rajan, E. Bordes, M. S. Strano, A. A. Padua and D. Blankschtein, *J. Phys. Chem. C*, 2017, **121**, 9022-9031.
12. B. Luan and R. Zhou, *Appl. Phys. Lett.*, 2016, **108**, 131601.
13. J.-W. Jiang, H. S. Park and T. Rabczuk, *J. Appl. Phys.*, 2013, **114**, 064307.

14. M. Dallavalle, N. Sändig and F. Zerbetto, *Langmuir*, 2012, **28**, 7393-7400.

15. V. Varshney, S. S. Patnaik, C. Muratore, A. K. Roy, A. A. Voevodin and B. L. Farmer, *Comput. Mater. Sci.*, 2010, **48**, 101-108.

16. T. Liang, S. R. Phillpot and S. B. Sinnott, *Phys. Rev. B*, 2009, **79**, 245110.

17. T. Onodera, Y. Morita, A. Suzuki, M. Koyama, H. Tsuboi, N. Hatakeyama, A. Endou, H. Takaba, M. Kubo and F. Dassenoy, *J. Phys. Chem. B*, 2009, **113**, 16526-16536.

18. Y. Morita, T. Onodera, A. Suzuki, R. Sahnoun, M. Koyama, H. Tsuboi, N. Hatakeyama, A. Endou, H. Takaba and M. Kubo, *Appl. Surf. Sci.*, 2008, **254**, 7618-7621.

19. U. Becker, K. M. Rosso, R. Weaver, M. Warren and M. F. Hochella Jr, *Geochim. Cosmochim. Acta*, 2003, **67**, 923-934.

20. P. Faye, E. Payen and D. Bougeard, *J. Chem. Soc., Faraday Trans.*, 1996, **92**, 2437-2443.

21. T. M. Brunier, M. G. Drew and P. C. Mitchell, *Mol. Simul.*, 1992, **9**, 143-159.

22. M. Drew, S. Edmondson, G. Forsyth, R. Hobson and P. Mitchell, *Catal. Today*, 1988, **2**, 633-641.

23. *CRC Handbook of Chemistry and Physics*, W. M. Haynes, Ed., CRC Press, Boca Raton, 2014.

24. E. Otyepková, P. Lazar, J. Luxa, K. Berka, K. Čépe, Z. Sofer, M. Pumera and M. Otyepka, *Nanoscale*, 2017, **9**, 19236-19244.

25. T. Björkman, A. Gulans, A. V. Krasheninnikov and R. M. Nieminen, *Phys. Rev. Lett.*, 2012, **108**, 235502.

26. J. Fuhr, J. Sofo and A. Saúl, *Phys. Rev. B*, 1999, **60**, 8343-8347.

27. K. Weiss and J. M. Phillips, *Phys. Rev. B*, 1976, **14**, 5392-5395.